Volume 1 | Number 1 | Jan 2013 | Pages 1–100

ChemComm

Chemical Communications
www.rsc.org/chemcomm

ROYAL SOCIETY OF CHEMISTRY

This is an *Accepted Manuscript*, which has been through the Royal Society of Chemistry peer review process and has been accepted for publication.

Accepted Manuscripts are published online shortly after acceptance, before technical editing, formatting and proof reading. Using this free service, authors can make their results available to the community, in citable form, before we publish the edited article. We will replace this *Accepted Manuscript* with the edited and formatted *Advance Article* as soon as it is available.

You can find more information about *Accepted Manuscripts* in the **Information for Authors**.

Please note that technical editing may introduce minor changes to the text and/or graphics, which may alter content. The journal's standard **Terms & Conditions** and the **Ethical guidelines** still apply. In no event shall the Royal Society of Chemistry be held responsible for any errors or omissions in this *Accepted Manuscript* or any consequences arising from the use of any information it contains.

ROYAL SOCIETY OF CHEMISTRY

www.rsc.org/chemcomm

Journal Name

COMMUNICATION

Self-organized nanoclusters in solution-processed mesoporous In-Ga-Zn-O thin films

C. Revenant,[a] M. Benwadih [b] and M. Maret[c]

Self-organized nanoclusters were obtained in annealed solution-processed In-Ga-Zn-O thin films. STEM and anomalous grazing incidence small-angle X-ray scattering (GISAXS) reveal the formation of nanometer-sized nanoclusters together with the spontaneous creation of a mesopore pattern.

Self-organization can be produced from phase separation of inorganic assembly. Increasing temperature favours diffusional phase separation yielding local composition fluctuations. Phase separation has been found in dilute magnetic semiconductor thin films,[1] in some oxide systems used to grow checkerboard films.[2] Surface-directed phase separation has been observed in hafnium silicate thin films elaborated by atomic layer deposition and characterized by a perpendicular composition wave.[3] All these films with structures originating from phase separation have been elaborated by solid-state deposition. Nevertheless, solution-processed inorganic thin films have been intensively developed, for example, to fabricate transparent conducting oxide (TCO) thin films, like In-Ga-Zn-O (IGZO).[4] The TCOs play a critical role in many current and emerging optoelectronic devices. In general, custom-made morphologies obtained by sol-gel techniques are extremely important for this field.[5] In sol-gel processing, annealing at high temperatures is needed to turn the gel film to an oxide compound through chemical reactions.[6] Previous work has shown that annealed IGZO films exhibit pores produced by the evaporation of residual organics.[7] However, tracking the influence of possible phase separation on self-organization remains an experimental challenge in mesoporous multimetallic oxide films. In this communication, we present the influence of the rapid thermal annealing on the nanoscale phase separation in nominally identical IGZO sol-gel films prepared on silicon wafers.

Figure 1 shows plane-view scanning electron microscope (SEM) images of IGZO films rapidly annealed up to 300, 380 and 450°C. A large density of self-assembled pores emerging at the film surface is observed. Large-scale pictures with a few hundreds of pores allowed
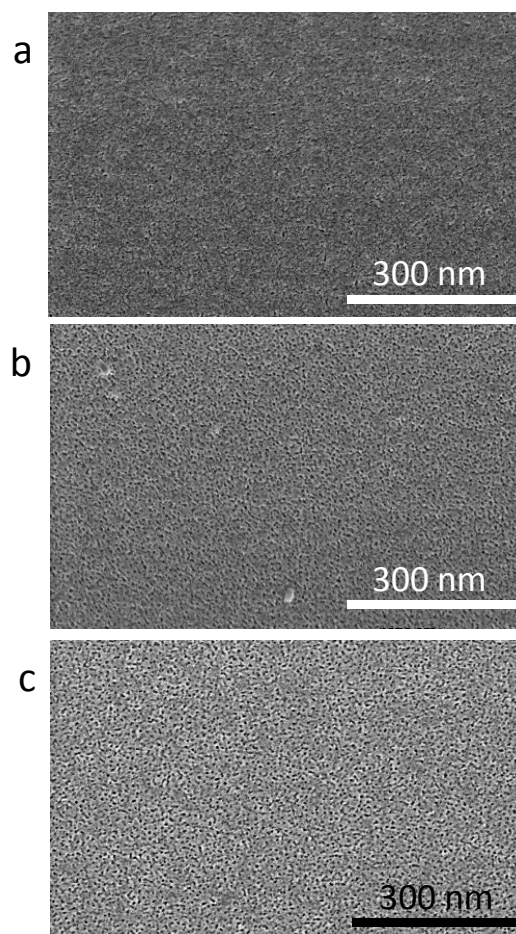
Fig. 1. Self-assembled pores at the IGZO film surface upon thermal annealing. Plane-view SEM images of IGZO films annealed up to 300°C (a), 380°C (b), and 450°C (c). The black areas correspond to pores.
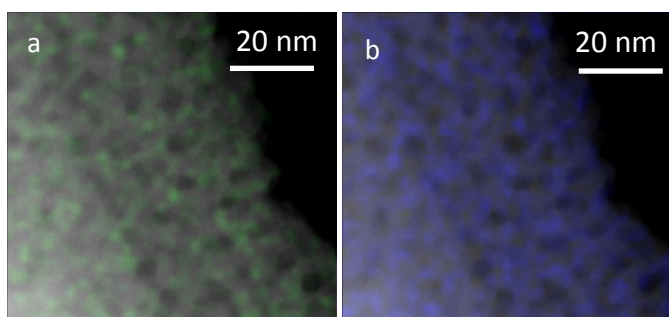
Fig. 2 Morphology of the IGZO film rapidly annealed at 450°C. EDX elemental mapping of Ga (a), and Zn (b). Each elemental mapping is superimposed on the HAADF-STEM image of the IGZO film. Dark areas correspond to pores.

to derive precisely the average pore size (Table 1). The average diameter ranges from 3 to 5 nm for an annealing temperature of 300

to 450°C, respectively. Moreover, high-angle annular dark field (HAADF) scanning transmission electron microscopy (STEM) has been performed on an IGZO film annealed at 450°C. In addition, we carried out local elemental mapping by energy dispersive X-ray spectroscopy (EDX) to address composition variation of Zn and Ga in the film annealed at 450°C. Both elemental maps are superimposed on the STEM image (Fig. 2). Pores are revealed inside the film. The elemental maps reveal the existence of self-assembled nanometer-sized Zn-rich and Ga-rich clusters. More precisely, the superimposed images reveal that Ga-rich clusters surround the pores, as Zn-rich clusters are in between the pores.

To deepen the morphological changes in the annealed films, we performed grazing incidence small-angle X-ray scattering (GISAXS)[8] measurements for samples rapidly annealed at temperatures of 300, 380, and 450°C (Fig. 3, first row). The X-ray penetration depth can be controlled by the incident angle. To achieve full penetration into the films, the incident angle was set to 0.3° (i.e. above the measured critical angle of the samples equal to 0.18°).
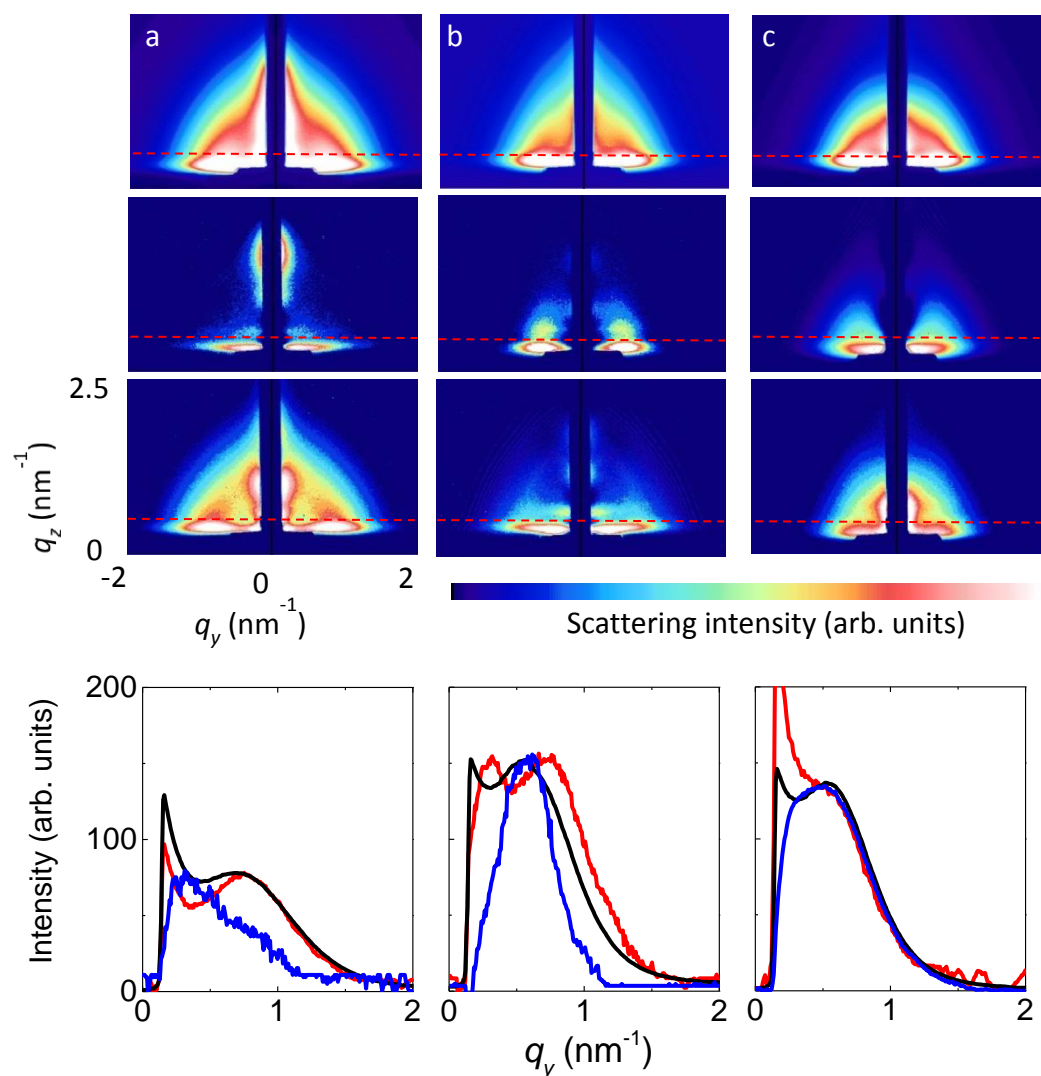
Fig. 3 X-ray scattering data of the IGZO film annealed at three different temperatures. GISAXS data (first row), AGISAXS data from the Zn-rich nanoclusters (second row), AGISAXS data from the Ga-rich nanoclusters (third row), normalized q_y linescans at $q_z = 0.5$ nm^{-1} (fourth row) for films annealed at 300°C (a), 380°C (b), and 450°C (c). In two-dimensional patterns, the red dot lines mark the position for horizontal cuts. The black curves represent the linescans extracted from the GISAXS data and the blue (red) ones those extracted from the AGISAXS data at the Zn (Ga) edges.

ChemComm Accepted Manuscript

Journal Name

COMMUNICATION

		Main morphological parameters (nm)							
T (°C)	Thin film thickness[a]	Microscopy	GISAXS			Zn		Ga	
		d_p	D_p	d_p	$D_{//}$	$D_\perp$	d	$D_{//}$	d
300	27±1	3±1	9±1	4.5±0.5	-	-	5±0.5	8.5±1	4.5±0.5
380	20±1	4±1	11±1	5.5±0.5	11±1	10±1	5.8±0.5	9±1	5.5±0.5
450	12±1	5±1	12±1	6±0.5	12±1	-	6±0.5	12±1	6±0.5

[a]The thickness of the thin film was measured from SEM cross-section images (see ESI).

Table 1. Morphology of the pores and of the nanoclusters. The GISAXS analysis is described in the ESI.

At 300°C (Fig. 3a, first row), the scattering signal occurring at small q_y (the momentum transfer parallel to the sample surface) and q_z (the momentum transfer perpendicular to the sample surface) comes mostly from the pores, due to their large electronic density contrast with respect to IGZO. Whatever the temperature, the GISAXS intensity shows an oblong spheroid shape corresponding to pores with an oblate spheroid shape (see GISAXS simulation in ESI). Indeed, simulations are powerful to distinguish between different shapes on the nanoscale.[9] As the annealing temperature increases, the shrinkage of the scattered intensity towards the origin of the reciprocal space corresponds to an increase in the pore size. The q_y linescans at q_z=0.5 nm^{-1} are shown in Figure 3 (fourth row) for the three temperatures. The pronounced in-plane peaks indicate strong in-plane spatial correlations between pores. As the temperature increases from 300 to 450°C, the average distance between the pores D_p, inversely proportional to the q_y position of the peak maximum, increases from 9 to 12 nm and the in-plane pore diameter d_p increases from 4.5 to 6 nm (Table 1). The pore diameters deduced from GISAXS are slightly larger than those extracted from the SEM images (Table 1). Indeed, in the case of a distribution of sizes, the GISAXS values may be overestimated,[10] as the GISAXS intensity is proportional to the square of the scatterer volume.

To probe nanoclusters within the annealed thin films and their possible spatial correlations, we performed anomalous GISAXS (AGISAXS) measurements in the vicinity of the K-edges of Zn and Ga. This technique allows separating the scattering from one type of cluster from the other contributions including other types of clusters, pores, surface roughness or defects.[11] At the Zn (Ga) edge, the spatial correlations between Zn (Ga)-rich clusters can thus be identified. The second (third) row of Figure 3 shows the AGISAXS patterns obtained at the Zn (Ga) edges for the three IGZO films. The corresponding q_y linescans at q_z=0.5 nm^{-1} are shown in Figure 3 (fourth row). At 300°C (Fig. 3a, second and third row), the emergence of a scattering signal at small q_y and q_z confirms the existence of Zn-rich and Ga-rich clusters. The intensity for Ga shows an oblong spheroid shape similar to that of the pores indicating that Ga-rich clusters have a symmetry similar to that of the pores. The AGISAXS and EDX observations suggest that the Ga clusters decorate the pores. Moreover, in-plane peaks at q_y=0.74 nm^{-1} indicate strong positional correlations between the Ga-rich clusters at a distance $D_{//}$ of 8.5 nm. At 380°C (Fig. 3b, second and third row), pronounced in-plane peaks for both contributions indicate strong in-plane correlations between the Zn-rich (resp. Ga-rich) clusters. For Zn, in-plane peaks at q_y=0.57 nm^{-1} indicate an in-plane distance $D_{//}$

of 11 nm, and the existence of an interference peak along q_z indicates strong out-of-plane correlations between Zn-rich clusters. The out-of-plane interference peak at q_z~0.6 nm^{-1} corresponds to an out-of-plane distance $D_\perp$ of 10 nm. At 380°C, the scattering curve in Fig. 3 for Ga widens and shows two peaks approximately at 0.7 and 0.35 nm^{-1}, corresponding to distances of approximately 9 and 18 nm. These peaks are situated on both sides of the scattering peak of the pores. The mean value of 9 nm may correspond to Ga facing each other on pore surfaces and that of 18 nm may correpond to Ga on opposite sides of pore surfaces (Fig. 4). The peak at small q_y seems to develop during annealing, leading finally to the smeared-out structure at 450°C, where only a shoulder is present at q_y=0.52 nm^{-1} corresponding to an in-plane distance $D_{//}$ of 12 nm (Fig. 3c, third row). This indicates larger distances between the Ga clusters. At 450°C (Fig. 3c, second row), the intensity for Zn shows approximately a spherical shape corresponding to spherical Zn-rich clusters. The persistence of the in-plane interference peak for Zn shows prevailing in-plane correlations between the Zn-rich clusters.
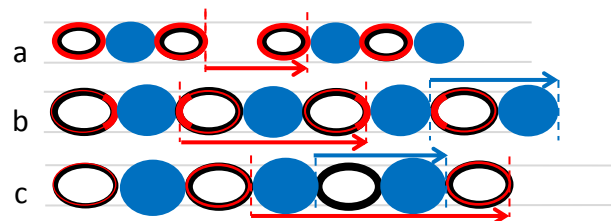
Fig. 4 Cross-section draft (from the linescans of Fig. 3) illustrating the morphology evolution parallel to the surface for the pores (black), the Zn clusters (blue), and the Ga clusters (red) at 300°C (a), 380°C (b), and 450°C (c). For the sake of simplicity, only a thin slab comprised of one layer of pores is represented. The arrows indicate the excursion distance L for the estimation of the diffusion coefficient D_c.

The cluster diameters d for Zn and Ga, estimated by AGISAXS, are similar to the pore diameters (Table 1). The Zn clusters show an opposite behavior than the Ga clusters. A broad distribution of Zn clusters at 300°C is present, which becomes more and more monodisperse at 380°C and polydisperse at 450°C. At 300 and 380°C, the Ga clusters are more closely packed than the Zn ones. In addition, peaks are present around the beamstop for Ga at 300 and 380°C as well as for Zn at 300°C, indicating a vertical ordering. The

period is approximately 9 nm (resp. 7 nm) at 300°C (resp. 380°C), which corresponds to the thickness of a single elaboration layer.

The morphology deduced from AGISAXS allows to deduce the diffusion coefficient for Zn and Ga. At 300°C, Ga diffuses on the distance between the pores. At 380°C, Ga may diffuse up to 18 nm (correponding to Ga on opposite sides of pore surfaces). At 450°C, Ga may diffuse on twice the distance between the pores. At 380°C and 450°C, Zn diffuses on a distance equal to that between the pores (11 nm and 12 nm, respectively). In one dimensional diffusion, the diffusion coefficient D_c is equal to $L^2/2 \times t$, where L is the average excursion distance and t is time. The annealing duration is 10 min. Diffusion constants have been estimated for Zn and Ga at different temperatures (Table 2). The diffusion coefficient of Ga is larger than that of Zn. The diffusion coefficient D_c as a function of temperature T is described by the Arrhenius relation, $D_c = D_0 e^{-E_a/RT}$ where E_a is the activation energy, D_0 is the pre-exponential coefficient and R is the gas constant. The Ga diffusion data from Table 2 display excellent Arrhenius behavior (Fig. S6, ESI). Linear fit of the data yields an activation energy for Ga of $(4.3 \pm 1) \times 10^4$ Jmol^{-1}.

T	Zn		Ga	
(°C)	L (nm)	D_c (nm^2 s^{-1})	L (nm)	D_c (nm^2 s^{-1})
300	-	-	8.5	0.06 ± 0.02
380	11	0.10 ± 0.02	18	0.27 ± 0.03
450	12	0.12 ± 0.02	24	0.48 ± 0.08

Table 2. Estimate of diffusion constants D_c of Zn and Ga. The parameter L is the excursion distance (cf. Fig. 4).

These mesoporous thin films have high surface-to-volume ratio. When surface area increases, the excess free energy ΔG has to be taken into account. It is equal to γ×S where S is the surface area and γ is the free energy per unit surface area. The surface area is comprised of the plane surface parallel to the substrate and of the pore surfaces. From the morphological data of the pores, the surface area can be estimated. At 450°C, a conservative estimate yields 50 m^{2}g^{-1}. Estimates of the surface energies are required to understand the nanostructure formation. Surface energies of oxides are mostly in the range 0.5-3.5 Jm^{-2}.[12] Relaxed surface energies of In$_2$O$_3$ are 1.76 Jm^{-2} for (100), 1.07 Jm^{-2} for (110), and 0.89 Jm^{-2} for (111) surface.[13] Anhydrous surface of wurtzite ZnO has surface energies of 2.55 Jm^{-2}.[14] Surface energies for relaxed β-Ga$_2$O$_3$ is in the range of 0.68-2.03 Jm^{-2} according to the orientation and reconstruction of the surface.[15] The fundamental understanding of the phase separation and of their assemblage relies on the energy minimization in this high surface area system. As the pores are created, the system will expose the lowest-energy phase at the surface, provided that diffusion allows to induce sufficient mass transport. According to the surface energy values of the three considered oxides, In$_2$O$_3$ and β-Ga$_2$O$_3$ are preferentially at the surface contrary to ZnO. The physical mechanism of self-organization of Ga nanoclusters can be understood as follows: it is proposed that during annealing Gallium oxide, highly mobile, aggregates into nanoclusters at the surface of the pores.

In conclusion, we have shown direct evidence of the nanocluster organization using STEM/EDX and GISAXS. Nanoclusters are not arranged in random but have a self-organization. The nanocluster organization in the annealed films is closely related to the pore arrangement in film. This phenomenon of self-organization can be explained by the minimization of surface energies. Our results on self-organized nanoclusters could be an excellent model for novel fundamental studies of nanoclusters in mesoporous matrix. The proposed synthesis approach represents a significant advance over other

processes that rely in incorporating functional materials into templates. The two basic approaches to creating patterns in a controlled and repeatable way are the top-down and bottom-up techniques. The former uses sophisticated tools like advanced lithography tools. On the contrary, bottom-up method like the one presented here, aims to organize constituents through inherent processes in the manipulated system. The advantages of our method are simplicity, large-scale processes even on flexible substrates, and cost-effectiveness. Our method relies on creating pores and using constituents with different surface energies. For a system with several constituents with different surface energies, the constituent with low surface energy will be very close to the pores. This method can be used, for example, in electronics, magnetism, thermoelectricity.

Notes and references

[a] Univ. Grenoble Alpes, INAC-SP2M, F-38000 Grenoble, France. CEA, INAC-SP2M, F-38000 Grenoble, France.
[b] Univ. Grenoble Alpes, LITEN, F-38000 Grenoble. CEA, LITEN, F-38000 Grenoble, France.
[c] Univ. Grenoble Alpes, SIMAP, F-38000 Grenoble. CNRS, SIMAP, F-38000 Grenoble, France.
Electronic supplementary information (ESI) available.

1   S. Kuroda, N. Nishizawa, K. Takita, M. Mitome, Y. Bando, K. Osuch and T. Dietl, *Nature materials*, 2007, **6**, 440; A. Wójcik, M. Godlewski, E. Guziewicz, K. Kopalko, R. Jakiela, M. Kiecana, M. Sawicki, M. Guziewicz, M. Putkonen, L. Niinistö, Y. Dumont and N. Keller, *Appl. Phys. Lett.*, 2007, **90**, 082502; H.-S. Kim, L. Bi, H. Paik, D.-J. Yang, Y. C. Park, G. F. Dionne and C. A. Ross, *Nano Lett.*, 2010, **10**, 597.

2   S. Park, Y. Horibe, T. Asada, L. S. Wielunski, N. Lee, P. L. Bonanno, S. M. O'Malley, A. A. Sirenko, A. Kazimirov, M. Tanimura, T. Gustafsson and S.-W. Cheong, *Nano Lett.*, 2008, **8**, 720; J. L. MacManus-Driscoll, P. Zerrer, H. Wang, H. Yang, J. Yoon, A. Fouchet, R. Yu, M. G. Blamire and Q. Jia, *Nature materials*, 2008, **7**, 314.

3   J. Liu, X. Wu, W. N. Lennard and D. Landheer, *Phys. Rev. B*, 2009, **80**, 041403(R).

4   R. M. Pasquarelli, D. S. Ginley and R. O'Hayre, *Chem. Soc. Rev.*, 2011, **40**, 5406.

5   K. Sarkar *et al.*, *ChemSusChem*, 2013, **6**, 1414.

6   L. L. Hench and J. K. West, *Chem. Rev.*, 1990, **90**, 33; D. B. Mitzi, *Solution Processing of Inorganic Materials*; Wiley: New Jersey, 2009.

7   H. Jeon, J. Song, S. Na, M. Moon, J. Lim, J. Joo, D. Jung, H. Kim, J. Noh and H.-J. Lee, *Thin Solid Films*, 2013, **540**, 31.

8   P. Müller-Buschbaum, *Anal. Bioanal. Chem*, 2003, **376**, 3.

9   M. Schwartzkopf *et al.*, *Nanoscale*, 2013, **5**, 5053; S. Yu *et al.*, *J. Phys. Chem. Lett.*, 2013, **4**, 3170.

10 V. Jousseaume, G. Rolland, D. Babonneau and J.-P. Simon, *Thin Solid Films*, 2009, **517**, 4413.

11 J.-P. Simon, D. Babonneau, M. Drouet and O. Lyon, *J. Appl. Cryst.*, 2009, **42**, 312.

12 A. Navrotsky, *ChemPhysChem*, 2011, **12**, 2207.

13 K. H. L. Zhang, A. Walsh, C. R. A. Catlow, V. K. Lazarov and R. G. Egdell, *Nano Lett.*, 2010, **10**, 3740.

14 P. Zhang, F. Xu, A. Navrotsky, J. S. Lee, S. Kim and J. Liu, *Chem. Mater.*, 2007, **19**, 5687.

15 V. M. Bermudez, *Chemical Physics*, 2006, **323**, 193.